Research Article

Katharina Frey*, Beatrice Zimmerling, Patrick Scheibe, Franziska G. Rauscher, Andreas Reichenbach, Mike Francke and Robert Brunner

Does the foveal shape influence the image formation in human eyes?

https://doi.org/10.1515/aot-2017-0043
Received May 24, 2017; accepted July 14, 2017; previously published online September 13, 2017

Abstract: In human eyes, the maximum visual acuity correlates locally with the fovea, a shallow depression in the retina. Previous examinations have been reduced to simple geometrical fovea models derived from postmortem preparations and considering only a few superficial ray propagation aspects. In the current study, an extended and realistic analysis of ray-optical simulations for a comprehensive anatomical realistic eye model for the anterior part and realistic aspherical human foveal topographical profiles deduced from *in vivo* optical coherence tomography (OCT) are presented, and the refractive index step at the transition from vitreous to retinal tissue is taken into account. The optical effect of a commonly shaped (averaged) and an extraordinarily shaped foveal pit were both compared to the analysis of an assumed pure spherical boundary layer. The influence of the aperture size, wavelength, and incident angle on the spot size and shape, as well as the axial focal and lateral centroid position is investigated, and a lateral displacement of about 2 µm and an axial shift of the best focal position of less than 4 µm are found. These findings indicate only small optical effects that are laterally in the range of inter-receptor distances and axially less than the photoreceptor outer segment dimension.

Keywords: concaviclivated foveal shape; human eye model; lateral and axial shift; ray-trace analysis; retinal image.

1 Introduction

A fovea, the retinal pitted invagination in the area centralis, is found in many vertebrates such as fish, reptiles, birds and in higher primates including humans. Because of the refractive index step between the retinal tissue and vitreous, the fovea defines an optically effective interface with aspherical characteristics, which influences the ray propagation to the receptor layer buried about 250 µm within the retinal layers [1]. In principle, two basic foveal shapes can be distinguished [2]. On the one hand, the convexiclivate type of fovea is a deep, funnel-shaped depression with a convex slope of the side walls and is observed in birds, some lizards, and certain deep-sea teleosts. On the other hand, the concaviclivate type of fovea is shallow and gradually shaped; the human fovea is of this type. Previous examinations on the influence of the fovea on the image-forming process have mainly been focused on the steep foveae types in which increasing magnification and directional-dependent distortion effects were predicted [3–7]. These investigations have been restricted to simple geometrical descriptions of the foveal shape, such as spheres and paraboloids. Real geometrical foveal structures from living creatures have not yet been examined. Moreover, the ray-trace considerations have been partly reduced to a few selected rays approaching the vitreo-retinal interface, and very limited numbers of incidence directions and wavelength-dependent effects have been

***Corresponding author: Katharina Frey,** Ernst-Abbe-Hochschule, University of Applied Sciences Jena, Carl-Zeiss-Promenade 2, 07745 Jena, Germany, e-mail: katharina.frey@eah-jena.de. http://orcid.org/0000-0003-0050-608X
Beatrice Zimmerling and Andreas Reichenbach: Paul Flechsig Institute for Brain Research, Department of Pathophysiology of Neuroglia, Leipzig University, Liebigstr. 19, 04103 Leipzig, Germany
Patrick Scheibe: Saxonian Incubator for Clinical Translation (SIKT), Leipzig University, Philipp-Rosenthal-Str. 55, 04103 Leipzig, Germany
Franziska G. Rauscher: Department of Ophthalmology, Leipzig University Hospital, Liebigstr. 10-14, 04103 Leipzig, Germany
Mike Francke: Paul Flechsig Institute for Brain Research, Department of Pathophysiology of Neuroglia, Leipzig University, Liebigstr. 19, 04103 Leipzig, Germany; and Saxonian Incubator for Clinical Translation (SIKT), Leipzig University, Philipp-Rosenthal-Str. 55, 04103 Leipzig, Germany
Robert Brunner: Ernst-Abbe-Hochschule, University of Applied Sciences Jena, Carl-Zeiss-Promenade 2, 07745 Jena, Germany; and Fraunhofer Institute for Applied Optics and Precision Engineering (IOF) Jena, Albert-Einstein-Str. 7, 07745 Jena, Germany

www.degruyter.com/aot

© 2017 THOSS Media and De Gruyter

Open Access. © 2017 Katharina Frey et al., published by De Gruyter. This work is licensed under the Creative Commons Attribution-NonCommercial-NoDerivatives 4.0 License.

Brought to you by | MPI fuer Kognitions- und Neurowissenschaften
Authenticated
Download Date | 10/18/19 1:40 PM

investigated. Studies on the refracting characteristics of human foveae types are even more rare [2, 8]. C. Ross analyzed the optical functionality of the foveae of tarsiers, neglecting the influence of the anterior part of the eye and regarding only position shifts of three single rays. This contribution aims to answer the question on whether a comprehensive human eye model, which takes all optical components and their aberrations into account, leads to more detailed findings. In particular, field- and wavelength-dependent influences on spot sizes and positions, based on actual ray-bundle-cones are considered, which allow the estimation of aberration effects. With the current investigation, we address this issue by combining a realistic anatomical model of the anterior parts of the eye with real human fovea geometries. For the anterior eye, the human eye model of Liou and Brennan [9], with a gradient index profile of the crystalline lens, was used. To investigate the influence of actual fovea geometries on image formation, two selected and different foveal shapes (average and extraordinary), based on *in vivo* optical coherence tomography (OCT) measurements of a human eye were used. We analyzed the ray-optical behavior and implemented additional considerations that involve the variation of the observed field position, pupil diameter, chromatic effects, and especially the imaging behavior of peripheral colors in the receptor plane when the primary color is focused on this theoretical surface. These simulations validate and expand the knowledge about the correlation between aperture size and real and theoretical spot size, the effect of the foveal shape on either spot size and axial spot position, and, finally, the lateral spot position and color dependency of the incident angle.

2 Optical simulation basis

As an optical simulation base, the established human eye model of Liou and Brennan was used [9]. The optical setup for this optical system for an aperture diameter of 3 mm is summarized in Table 1.

This basic model includes aspheric shapes for all optical surfaces, which can be derived from Eq. (1), a gradient refractive index distribution for the crystalline lens [see Eq. (2)], and dispersion properties of the optical components [10, 11].

$$z(r) = \frac{r^2}{R + \sqrt{R - (1+k)c^2 r^2}}. \quad (1)$$

With c as the curvature value, 1/Radius, (mm^{-1}), k as the conic constant for the surface, r as the distance from the optical axis (mm). The gradient index distribution (GRAD A and GRAD P) within the eye lens for a special wavelength of 555 nm can be derived according to the following Eq. (2) from Ref. [9], with z as the distance along the optical axis to the apex and w as the distance in the lateral direction:

$$n(w, z) = n_{00} + n_{01} z + n_{02} z^2 + n_{10} w^2, \quad (2)$$

where $n_{00} = 1.368$, $n_{01} = 0.049057$, $n_{02} = -0.015427$, $n_{10} = -0.001978$ for the anterior part of the eye lens (GRAD A) and $n_{00} = 1.407$, $n_{01} = 0.00000$, $n_{02} = -0.006605$, $n_{10} = -0.001978$ for the posterior part (GRAD P). The refractive indices $n_{00}(\lambda)$ for other wavelengths beside 555 nm can be calculated with the following formula [11]:

$$n_{00}(\lambda) = n_{00}(@555\ \text{nm}) + 0.0512 - 0.14555\lambda + 0.0961\lambda^2. \quad (3)$$

In the original Liou-Brennan model, the retinal surface is assumed to be a pure spherical surface with a radius of curvature of 12 mm, and the physiological fact that the light-detecting photoreceptor layer is buried below the interface between the vitreous body and the top retinal layer is neglected.

In our approach, an optically homogeneous tissue with a thickness of 250 µm and a refractive index of $n_{retina} = 1.370$ at 555 nm wavelength with an Abbe's number of 50.23 was assumed for the retinal layer [1, 12]. Thus, the length of the vitreous was reduced accordingly. Although the retinal structure consists of several layers, the assumption of a homogeneous layer is reasonable, as the variation of the inter-retinal refractive index is much

Table 1: Liou Brennan eye model.

Surface	Name	Radius (mm)	Thickness (mm)	Refractive index at 555 nm	Conic constant *k*
1	Cornea	7.770	0.50	1.376	−0.18
2	Anterior chamber	6.400	3.16	1.336	−0.60
3	Eye lens: cortex	12.400	1.59	GRAD A	−0.94
4		Infinity	2.43	GRAD P	
5	Vitreous	−8.100	16.27	1.336	+0.96
6	Retina	−12.00	–	–	–

Brought to you by | MPI fuer Kognitions- und Neurowissenschaften
Authenticated
Download Date | 10/18/19 1:40 PM

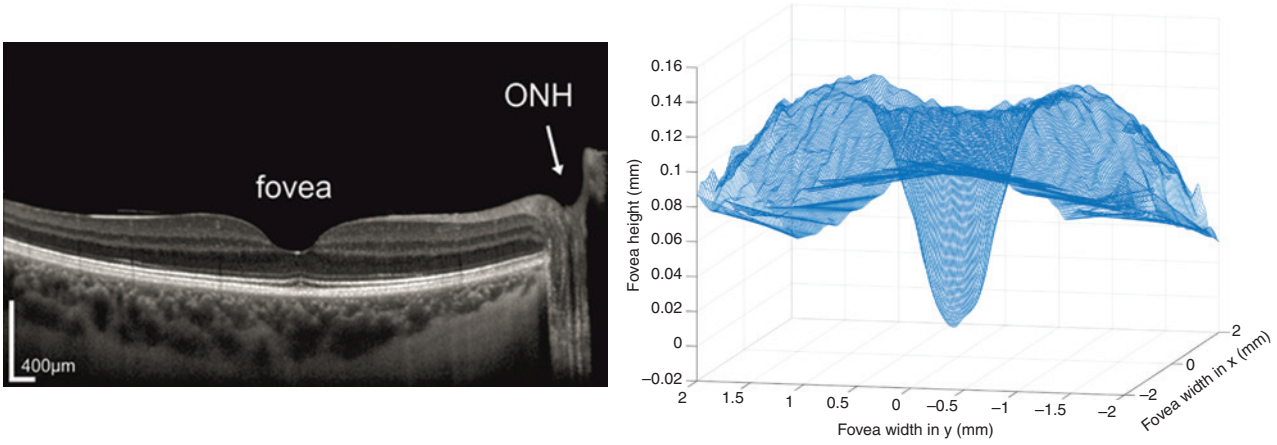

Figure 1: Cross-section of the fovea of a healthy eye (left image) obtained by an optical coherent tomography system (Heidelberg Spectralis SD-OCT). For a pronounced presentation, the axial direction is magnified with respect to the lateral direction. The inclination on the right side (left image) indicates the optic nerve head (ONH). On the right image, a mesh-diagram of a three-dimensional shape of the fovea region is shown.

smaller compared to the index step at the transition layer at the vitreo-retinal boundary [13]. The foveal shape was obtained from measurements of the retinal topography by Optical Coherence Tomography (OCT) (Heidelberg Spectralis SD-OCT, Germany).

Figure 1 shows, on the left side, the OCT cross-section of a healthy left human eye and, on the right side, the corresponding mesh-diagram of the three-dimensional foveal region. The depicted topography covers an extension of 4 mm in both lateral dimensions and a height variation of about 140 µm.

In previous researches the foveal shape was limited to simple geometrical descriptions such as spheres and paraboloids. This approach is restricted for distinct foveal zones and simple shapes. For our optical analysis, both an average and an extraordinary foveal form were used, which are depicted in Figure 2, as well as a pure spherical reference foveal shape with a radius of curvature of 11.63 mm and a thickness of 350 µm. The extraordinary form was transferred from Ref. [14]. For all three cases, the thickness of the vitreous was adapted such that the overall length of the optical system remained constant.

To use the measured topographical data of the fovea for optical analysis, we fitted the cross-section to a rotation-symmetric aspheric equation [15], with c as the curvature value (mm^{-1}), k as the conic constant for the surface, r as the distance from the optical axis (mm), and A_{2i} as the aspheric coefficients according to the following formula:

$$z(r)=\frac{cr^2}{1+\sqrt{1-(1+k)c^2r^2}}+\sum_{i=1}^{N}A_{2i}r^i. \qquad (4)$$

For the two different foveal shapes, the following parameters were determined (Table 2):

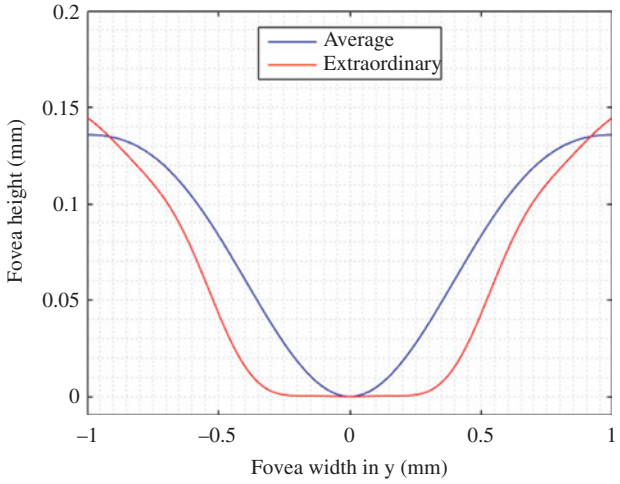

Figure 2: Comparison of different foveal shapes; in blue, the cross-section from the OCT measurements of an average foveal shape and, in red, a cross-section of an extraordinary foveal shape found in literature [14].

The quality of the fit for the average foveal shape is not significantly improved for aspheric coefficients of higher order than A_{12}; thus, they can be ignored. The presented fits are valid up to a diameter of 3 mm, which covers the main area of the fovea. As we are primarily interested in the influence of the foveal shape on image formation, this rotation-symmetric approach is reasonable.

From both model contributions, namely, the model of the anterior part of the eye and the optical model of the foveal shape, a combined overall model is now composed. For the comprehensive optical analysis, the dependency on several parameters, such as wavelength, aperture diameter, or the angle of incident ray bundles, were investigated

Brought to you by | MPI fuer Kognitions- und Neurowissenschaften
Authenticated
Download Date | 10/18/19 1:40 PM

Table 2: Aspheric parameter.

Parameter for i = 1–13	Average foveal shape	Extraordinary foveal shape
c	−1.14	−0.14
k	−7.29	−32.52
A_{02}	–	–
A_{04}	0.19	1.25
A_{06}	−0.11	−21.9
A_{08}	0.03	101.5
A_{10}	−2.5e − 3	−245.6
A_{12}	–	368.0
A_{14}	–	−365.9
A_{16}	–	248.7
A_{18}	–	−116.2
A_{20}	–	36.7
A_{22}	–	−7.50
A_{24}	–	0.89
A_{26}	–	−0.05

with the optical simulation program ZEMAX (Zemax LLC, Seattle, WA, USA) [15]. The essential evaluation criteria were the extent of the image spots and their centroid position for different imaging situations.

3 Simulation results

In the first simulation series, the influence of the aperture diameter on the imaging properties was investigated. This analysis also serves as a suitability proof to verify the applicability of our model approach. Depending on the light condition and object distances of the scene to be observed, the human pupil diameter varies between a minimum of 2 mm and a maximum of 8 mm [16]. In our model, the variation of the aperture size shows the highest performance and minimum spot size in the detector plane at a diameter of 4 mm, which corresponds well to literature values [17]. This size offers the best balance between minimizing diffraction effects by increasing the aperture and reducing aberrations by decreasing the opening diameter, respectively [18]. The found value for the depth of focus (DOF) for this setting correlates to the length of the light-receptive part of a photoreceptor cell [19]. The obtained results for the balancing diameter of 4 mm and the extension of the DOF shows that the introduced model is a valid base for further investigations.

3.1 Introduction to the simulation setup

The influence of the foveal topography on image formation for the two different exemplary structures is compared to a pure spherical boundary layer. The difference in shapes is depicted in Figure 3 (an average form (A) based on *in vivo* OCT measurements, an extraordinary shape (B) derived from literature [14]). The blue curves depict the respective foveal shapes, the red curves represent the spherical reference foveal shape, and the green curves shows the shape of the image layer. The y-axis indicates the fovea height in mm, and the x-axis the width in mm.

When an extended object is observed, the ray bundles originating from each object point enter the

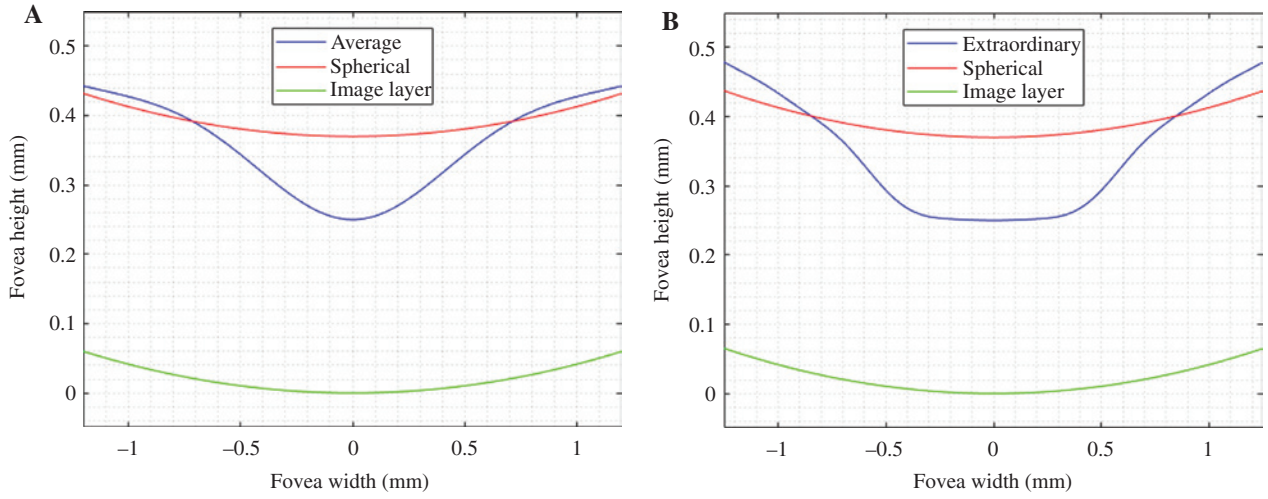

Figure 3: Comparison of different foveal shapes (blue), a simple spherical vitreo-retinal boundary (red), and the image layer shape (green). On the left side, an average foveal shape based on *in vivo* measurements (A) and, on the right side, an extraordinary shape (B) derived from literature [14] is shown.

Brought to you by | MPI fuer Kognitions- und Neurowissenschaften
Authenticated
Download Date | 10/18/19 1:40 PM

eye from various incoming directions. In particular, for larger object distances (infinite object distance), bundles of parallel rays enter the eye at different angles, in which each bundle is associated with a specific observation direction. These parallel ray bundles are imaged by the optical components to different positions on the receptor surface, creating an overall image of the observed scene. To investigate the influence of the foveal shape on the image-forming process, the ray trace for several ray bundles corresponding to different observation angles is simulated. For each incoming ray bundle, the resulting spot position and spot size on the image surface were calculated. The incident angle ranges from 0° to 3.2° to cover the foveal area of interest. The ray bundles belonging to the different angles pass through the aperture stop. Figure 4 shows the ray trace for all three cases ['average' (top), extraordinary (center) and spherical reference (bottom)] that takes the whole eye into account. The anterior part stays mainly the same, beside a slight adaption of the front surface of the eye lens; 13.05 mm (top), 13.02 mm (middle), and 13.03 mm (bottom). In the left column, the overall view is displayed; on the right column, a magnified view of the foveal region is displayed in more detail.

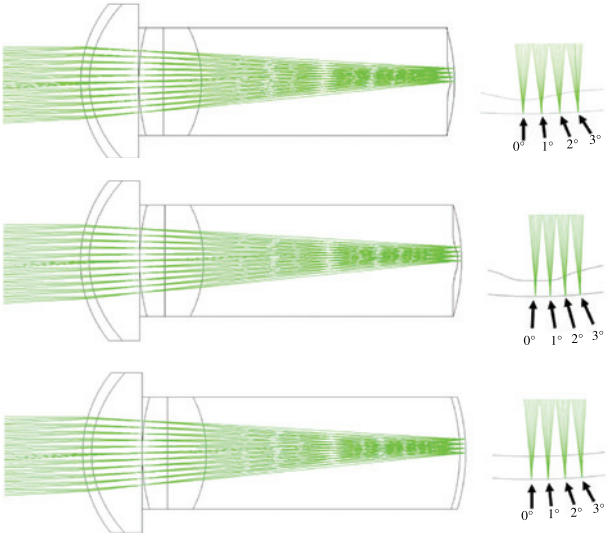

Figure 4: Comparison of the lateral image-forming process between the real case of an average foveal-shaped border surface (top), an extraordinary shape (middle), and the reference system of an assumed artificial spherical boundary layer of homogeneous thickness (bottom). On the left, the ray-trace overlaid on the comprehensive eye model for all cases is shown, while the right displays an extended view of the incoming ray bundles at the receptor layer for the different incident angles. The anterior part stays mainly the same, beside a slight adaption of the front surface of the eye lens; 13.05 mm (top), 13.02 mm (middle), and 13.03 mm (bottom).

For the qualitative and quantitative evaluation of the influence of different foveal shapes, these simulations are compared with the anterior eye model with a pure spherical fovea topography with a matched layer of homogeneous thickness [350 µm above the image layer (see Figure 4 bottom)].

3.2 Influence of incident angle on spot size

In the first analysis, the root-mean-square (RMS) spot sizes were compared for different incoming angles (0° to 3.2°) and wavelengths (555, 486 and 656 nm). The aperture was set to a diameter of 4 mm, which correlates to normal illumination conditions [20] and offers highest resolution. In each of the simulations, the radius of curvature or the front surface of the eye lens was adapted to three different target wavelengths for this configuration with a 4-mm aperture diameter, so that a minimum spot size for the specified wavelength was achieved on the image surface.

For a field-dependent comparison of shapes and sizes of the spot diagrams, the three different configurations depicted in Figure 4 were simulated for different incoming angles (Figure 5). For a representative situation and for all configurations, each radius of curvature for the eye lens was adapted as mentioned above, so

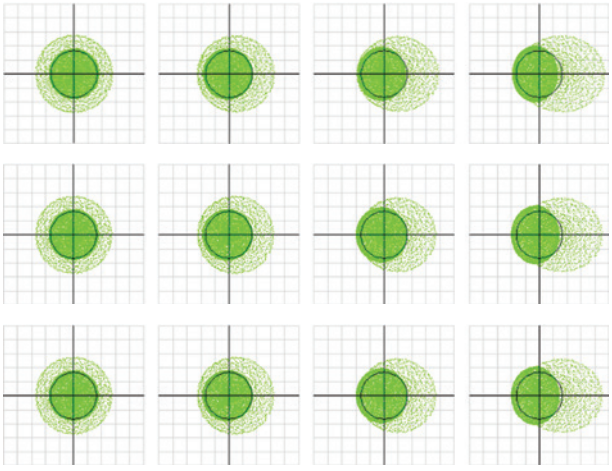

Figure 5: Field-dependent spot diagrams compared between a foveal-shaped retina and a homogeneous spherical receptor layer. For both configurations, the lens curvature was adapted so that the wavelength of 555 nm was in best focus in the receptor plane (represent in an enlarged 15-µmm scale diagram). The upper row corresponds to the average foveal-shaped retina, the middle row corresponds to the extraordinary foveal shape, and the lower row displays the result for the homogeneous spherical receptor layer. The black circles indicate the diffraction limit.

Brought to you by | MPI fuer Kognitions- und Neurowissenschaften
Authenticated
Download Date | 10/18/19 1:40 PM

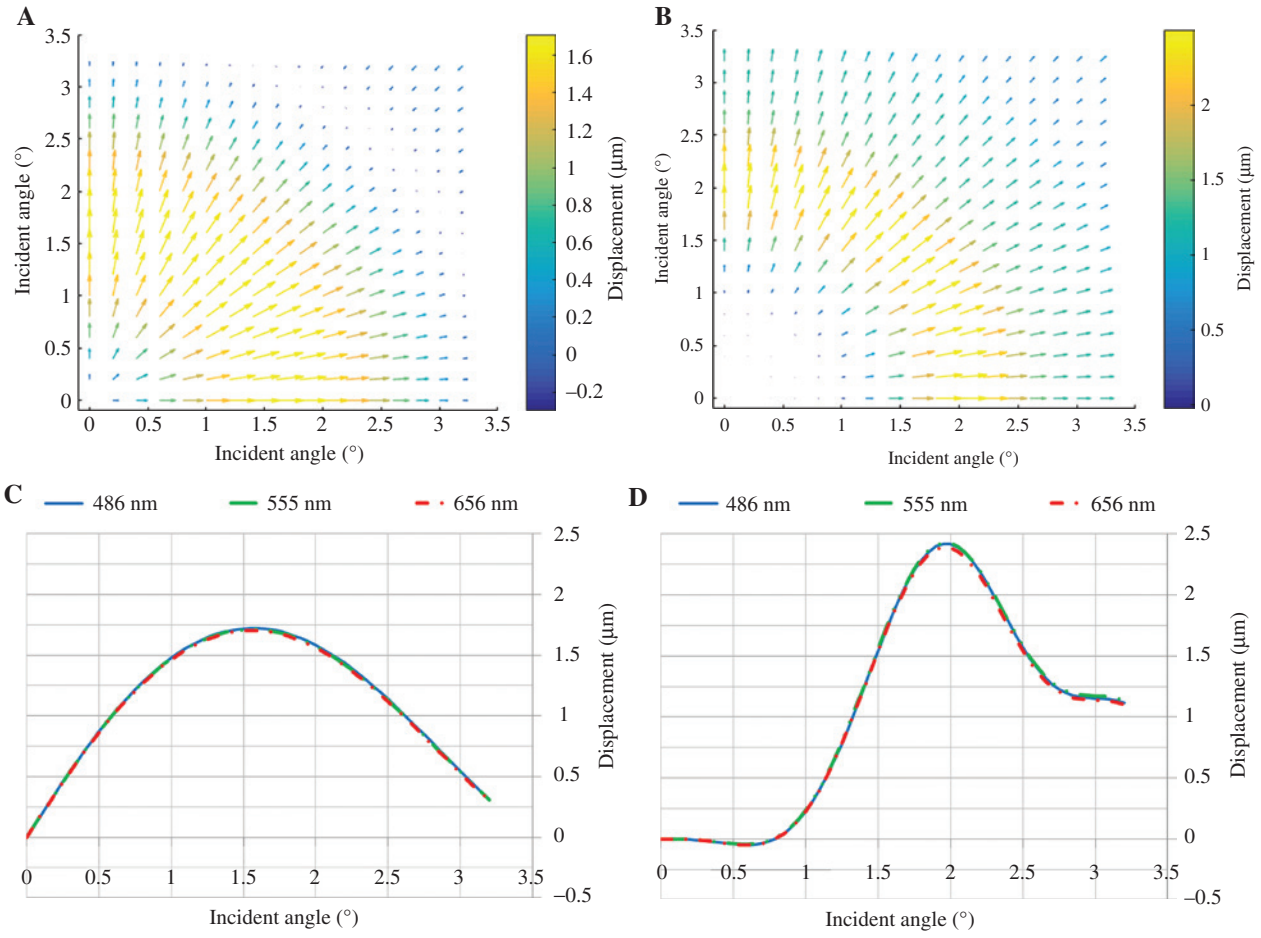

Figure 6: Lateral displacement of centroid position caused by the foveal shape in comparison to a homogeneous layer setup (target wavelength 555 nm, aperture diameter 4 mm) for the average foveal shape on the left side and for the extraordinary shape on the right side. (A) and (B) An arrow map; the length and the direction of the arrows indicate the strength and direction of the calculated displacement. (C) and (E) A radial cross-sectional display of the centroid displacement for an aperture diameter of 4 mm and for different wavelengths (486 nm, 555 nm, and 656 nm). The maximum displacement was found to be in the range of 1.75 µm.

that the wavelength of 555 nm was in best focus in the receptor plane (represent in an enlarged 15 µm scale spot diagram). The upper row corresponds to the foveal-shaped retina forms, the average and extraordinary concaviclivate fovea, while the lower row displays the result for a pure spherical vitreo-retinal boundary surface. The black circles indicate the diffraction limit. With increasing incident angle, the shape of the spot is becoming more asymmetric.

As a result of the comparison, the difference in form and size of the corresponding spot diagrams with and without fovea is negligible. For the target wavelength of 555 nm and for both foveal shapes (average and extraordinary) a RMS spot diameter of 4.2 µm was found at the central position and only marginally larger for 3.2° (4.8 µm). The same result also occurred for similar spot diagrams, for which another wavelength was selected as the target wavelength (not shown).

3.3 Influence of incident angle on centroid position

The second aspect of the comparison concerned the lateral displacement of the centroid positions of the spot distributions for the two cases (average and extraordinary). Here, the displacement is calculated as the lateral offset between the centroid positions for the case of a structured fovea and the corresponding positions of an assumed pure spherical boundary layer. In Figure 6, the lateral displacement for the average foveal shape on the left side, (A) and (C), and for the extraordinary shape on the right side, (B) and (D), is depicted as dependent on the incident angle (up to 3.2°). Again, a target wavelength of 555 nm and an aperture diameter of 4 mm were assumed. In the upper row, the displacement is presented in a color-coded arrow map in which the length and the direction of the arrows indicate the strength and direction of the

Brought to you by | MPI fuer Kognitions- und Neurowissenschaften
Authenticated
Download Date | 10/18/19 1:40 PM

calculated displacement. To enhance visualization, the color scales for average fovea (Figure 6A) and extraordinary shape (Figure 6B) are normalized differently.

The diagrams show that the transition between the rise and fall of the topography is reflected by the change in displacement direction and depicted by an inversion of the arrow directions. In particular, in the inner part of the fovea, the displacement points away from the center, and in the outer region, the displacement is inverted and oriented toward the center. The maximum displacement associated with the average foveal shape in comparison to an assumed pure spherical boundary layer was found to be in the average foveal shape in the range of 1.75 µm and, respectively, 2.5 µm for the extraordinary foveal shape independent of wavelength variation. In comparison to the size of the detecting unit (diameter of the outer segment of a cone is approximately 1–1.5 µm in the central foveal region [19]), it appeared that a small magnification effect could be attributed to the presence of the foveal shape. However, the effect, also regarding the RMS spot size of 4 µm for this configurations, is negligible as well as the difference between the average and extraordinary foveal shape.

Furthermore, it was found that a variation of wavelength had only a slight impact on the calculated displacement. This finding can be shown in the lower row of Figure 6, in which the diagrams (C) and (D) depict the corresponding centroid displacement for the three different target wavelengths (486 nm, 555 nm and 656 nm). For these investigations, it was again necessary to adapt the lens radius of curvature for each target wavelength (for the average, extreme and spherical boundary layer for a wavelength of 486 nm to 15.42 mm, 15.38 mm and 15.40 mm, for 555 nm to 13.05 mm, 13.02 mm and 13.03 mm and for 656 nm respectively to 11.55 mm, 11.53 mm, and 11.54 mm) so that the best focus was observed in the receptor plane. For all combinations of varying target wavelengths, the maximum calculated change in the displacement was smaller than 100 nm between the compared parameter. As an example, Figure 6C and D shows a radial cross-sectional representation of the displacement as a function of the incidence angle for different wavelengths and an aperture diameter of 4 mm. All displayed curves coincide almost exactly.

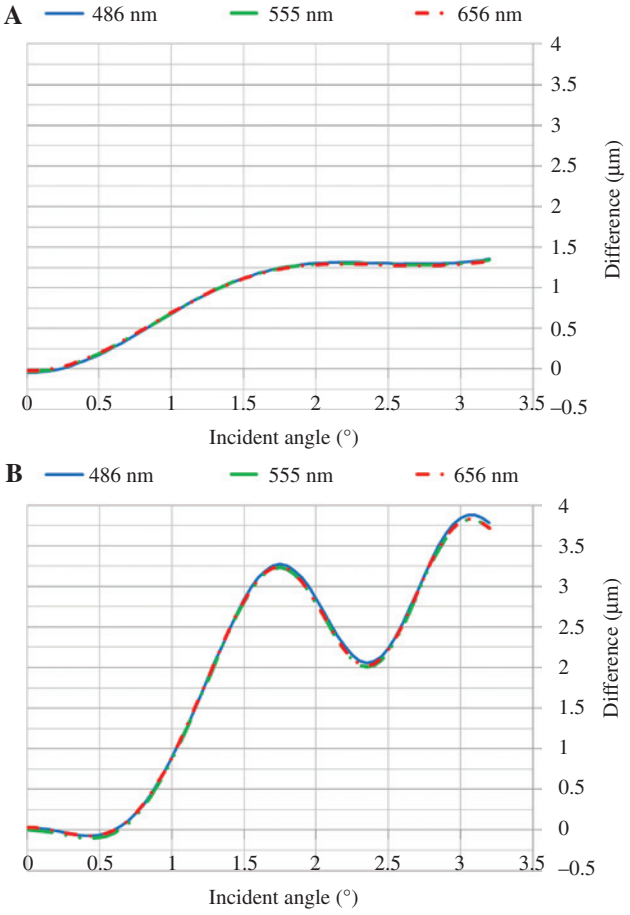

Figure 7: Difference of the axial position of the centroid for a target wavelength of 555 nm and an aperture diameter of 4 mm. (A) The results for an average foveal-shaped vs. a spherical vitreo-retina boundary, (B) for the extraordinary foveal shape vs. the spherical boundary layer for three different target wavelengths (486 nm, 555 nm and 656 nm).

3.4 Effects of the foveal shape on the axial focal position

In addition to the lateral position of the centroid of the spot for the two cases (average respectively extraordinary foveal shape vs. pure spherical shape), its axial dependency was also considered. Again, an aperture diameter of 4 mm was assumed. In an initial step for the three cases, the geometry of the crystalline lens was adjusted again to the values mentioned above, so that the best focal position for the centroid fell in the receptor layer when assuming a 0° incidence angle.

The results are depicted in Figure 7, where the difference of the axial position of the centroid, defined as the minimum RMS diameter of the ray bundle, is displayed for each target wavelength as a function of the incidence angle. The axial difference is again calculated from the centroid positions for the respective foveal structure and compared to the case of an assumed homogeneous layer. The difference in focus shift, comparing the three different target wavelengths, is negligible, as well as the influence of the incident angle. Although the values between the different setups (average vs. spherical and extraordinary vs. spherical) vary slightly, the overall difference

Brought to you by | MPI fuer Kognitions- und Neurowissenschaften
Authenticated
Download Date | 10/18/19 1:40 PM

is, nevertheless, negligible. Furthermore, the axial positions for the other none-target wavelengths were determined. From these values, the maximum axial distance between the red and blue focal position was calculated using the ray-tracing. It was found that the axial spectral spread between the different focal positions was larger than 180 µm for all single configurations. That means, the focus of a certain wavelength (i.e. green) is 180 µm away from another wavelength (e.g. blue or red) in the axial direction. However, the different foveal shape has only an insignificant influence on this behavior.

The observable angle dependency was found to be rather small in comparison to the overall spectral spread, 1.5 µm, respectively, 4 µm compared to 180 µm. From these calculations, it follows that the foveal shape of the retina offers only a minor direct significant influence with respect to the axial resolution compared to the situation of a pure spherical boundary layer.

4 Conclusion

The authors of this presented work calculated, in a comprehensive optical system, the anterior part of a human eye combined with the two different foveal structures as well as their possible optical functions. Optical simulations regarding aperture sizes, wavelength variation, and incident angles were carried out for a setup with the average and the extraordinary foveal shapes, as well as for an optical system with a spherical vitreo-retinal boundary layer. The simulation results were compared to analyze the actual influence of the foveal shape. The findings showed that the foveal shape has no significant influence on the spot size or form during imaging. However, the behavior of the lateral displacement clearly reflecting the actual foveal shape, which is in the range of a cone size (about 2 µm) for either form, thereby, indicating a direct influence of its slope on image projection. A lateral displacement of an image by one or two cone-outer-segments respectively pixels may particularly improve the visible acuity, which requires a different illumination of three adjacent cones. The influence could also be seen in the axial focal position over aperture sizes or wavelength but, in this case, was vanishingly small compared to the overall dispersion effect. In summary, we show that the influence of the foveal shape has an impact on the image distribution among the foveal cones. Although the ray-tracing results of our model of the human eye indicate an optical effect of the concaviclivate foveal structure, even with an extraordinary foveal shape, the influence is yet small. A major magnifying optical effect, as suggested for a convexiclivate fovea, however, could be definitely excluded. Possible physiological relevance for these effects has to be determined in future work.

Acknowledgment: K. Frey expresses thanks to the Ernst-Abbe-Hochschule Jena for the possibility to take part in the Ph.D. program of the University. This work was supported by Deutsche Forschungsgemeinschaft (Priority programme SPP 1757- FR 1825/1-1 to M.F. and A.R.; and GRK 1097/2 to A.R.), the Bundesministerium für Bildung und Forschung, BMBF (031A574B to M.F.), the Fraunhofer Gesellschaft in Germany within the cooperation program Fachhochschulen (project 'MIRO'), and the Thuringian Ministry for Economic Affairs, Science and Digital Society for the grant 'proMIRO' (FKZ 2015 – 0024).

References

[1] P. Scheibe, M. T. Zocher, M. Francke and F. G. Rauscher, Exp. Eye Res. 148, 1–11 (2016).
[2] G. L. Walls, 'The Vertebrate Eye and its Adaptive Radiation' (Cranbook Institute of Science, Bloomfield Hills, Michigan, 1942).
[3] R. J. Pumphrey, J. Exp. Biol. 25, 299–312 (1948).
[4] A. W. Snyder and W. H. Miller, Nature 275, 127–129 (1978).
[5] L. Harkness and H. C. Bennet-Clark, Nature 272, 814–816 (1978).
[6] S. Steenstrup and O. Munk, Optica Acta 27, 949–964 (1980).
[7] N. A. Locket, J. Ophthalmol. 20, 281–295 (1992).
[8] C. F. Ross and R. F. Kay, in 'Anthroid Origins New Visions' (Springer, USA, 2004).
[9] H.-L. Liou and N. A. Brennan, J. Opt. Soc. Am. 14, 1684–1695 (1997).
[10] J. G. Sivak and T. Mandelman, Vision Research 23, 1555–1559 (1982).
[11] D. A. Atchison and G. Smith, J. Opt. Soc. Am. 22, 29–37 (2005).
[12] M. Wagner-Schuman, A. M. Dubis, R. N. Nordgren, Y. Lei, D. Odell, et al., Investig. Ophthalmol. Vis. Sci. 52, 625–634 (2011).
[13] E. Chen, Ophthalmic Res. 25, 65–68 (1993).
[14] S. Tick, F. Rossant, I. Ghorbel, A. Gaudric, J.-A. Sabel, et al., Investig. Ophthalmol. Vis. Sci. 25, 5105–5110 (2011).
[15] Z. LLC, Zemax 13 Optical Design Program User's Manual. Radiant Zemax, June 2015.
[16] A. B. Watson and I. J. Yellot, J. Vis. 12, 1–16 (2012).
[17] H. Gross, F. Blechinger and B. Achtner, 'Handbook of Optical Systems, Volume 4: Survey of Optical Instruments' (Wiley-VCH, Weinheim, Germany, 2008).
[18] R. E. Fischer, B. Tadic-Galeb and P. R. Yoder, 'Optical System Design', 2nd ed. (McGraw-Hill, New York, USA, 2008).
[19] C. Youdelis and A. Nendrickson, Vis. Res. 26, 847–855 (1986).
[20] H. Goersch, 'Handbuch für Augenoptik', 4. ed. (Mauer Druck + Verlag, Geislingen, Deutschland, 2000).

Brought to you by | MPI fuer Kognitions- und Neurowissenschaften
Authenticated
Download Date | 10/18/19 1:40 PM